Dalton Transactions

ROYAL SOCIETY OF CHEMISTRY

PAPER

View Article Online
View Journal | View Issue

Cite this: *Dalton Trans.*, 2024, **53**, 15501

Annealing 1,2,4-triazine to iridium(III) complexes induces luminogenic behaviour in bioorthogonal reactions with strained alkynes†

Lydia Cooke,[a] Katie Gristwood,[b] Kate Adamson,[a] Mark T. Sims,[a] Michael E. Deary,[a] Dawn Bruce,[a] Antony N. Antoniou,[a] Hannah R. Walden,[a] James C. Knight,[b] Timothé Antoine-Brunet,[c] Marie Joly,[c] David Goyard,[c] Pierre-Henri Lanoë,[c] Nathalie Berthet[c] and Valery N. Kozhevnikov *[a]

Received 22nd May 2024,
Accepted 26th August 2024

DOI: 10.1039/d4dt01499e

rsc.li/dalton

A phenanthroline-type ligand containing an annealed 1,2,4-triazine ring was used to prepare novel Ir(III) complexes **3** and **4**. The complexes are non-luminescent but show luminogenic behaviour following the inverse electron demand Diels–Alder (IEDDA) reaction with bicyclononyne (BCN) derivatives. It was observed that the complexes react with **BCN-C10** faster than the corresponding free ligands. The magnitude of this accelerating metal-coordination effect, however, is less profound than in previously reported Ir(III) complexes of 1,2,4-triazines, in which the triazine was directly coordinated to the Ir(III) metal centre. Nevertheless, luminogenic behaviour opens prospects for the use of such complexes in bioimaging applications, which was demonstrated by developing a convenient methodology using the "chemistry on the complex" concept for labelling antibodies with luminescent Ir(III) complexes. The bioorthogonal reactivity of complex **4** was demonstrated by metabolically labelling live cells with BCN groups, followed by a luminogenic IEDDA reaction with the triazine iridium complex.

Introduction

Bioorthogonal chemistry emerged as a powerful tool in luminescence bioimaging that relies on the use of luminescent click reagents. Some of these probes demonstrate 'switch-on' luminescence following a conjugation reaction.[1–4] Luminogenic probes are highly desirable, as the non-conjugated probe generates no luminescent background, ensuring high sensitivity of the probe without the need for laborious washing protocols. Phosphorescent cyclometallated iridium(III) complexes enrich the field of luminescence bioimaging by offering unique characteristics and several advantages over traditional organic probes.[5,6] They are easy to prepare, highly tuneable, and photostable, and their long lived excited states provide opportunity for time-delayed elimination of the background luminescence as well as for luminescence lifetime imaging.[7] The interaction of the complexes in the excited state with oxygen is of interest for intracellular and *in vivo* oxygen sensing due to their oxygen-dependent emissions,[8,9] while sensitisation of singlet oxygen is utilised in photodynamic therapy.[10] In addition to luminescence, the presence of the heavy metal centre allows the use of additional complementary detection techniques such as X-ray fluorescence, ICP-MS and electron microscopy.[11,12]

Phosphorescent cyclometallated iridium(III) complexes were developed as bioorthogonal reagents incorporating a variety of click groups.[3] The inverse electron demand Diels–Alder (IEDDA) reaction is the fastest in the repertoire of bioorthogonal chemistry[13] and several examples of metal complexes have been reported in the literature.[14] Of particular interest are complexes in which the coordination of the Ir(III) metal centre to the diene facilitates the reaction kinetics. For example, Lo *et al.* demonstrated this effect in tetrazine complexes,[4] while we describe similar behaviour of Ir(III) complexes of 1,2,4-triazines.[15,16] Importantly, both the tetrazine and the triazine systems also show luminogenic behaviour in reactions with BCN derivatives.[4,15]

Here, we report the synthesis and evaluation of novel iridium(III) complexes that can participate in the IEDDA reaction. The novelty of these complexes arises from the 1,2,4-triazine fragment that is annealed to a phenanthroline-type

[a]*Department of Applied Sciences, Northumbria University, Ellison Building, Newcastle upon Tyne, NE1 8ST, UK. E-mail: valery.kozhevnikov@northumbria.ac.uk*
[b]*School of Natural and Environmental Sciences, Newcastle University, Bedson Building, Newcastle upon Tyne NE1 7RU, UK*
[c]*Université Grenoble Alpes, CNRS, DCM UMR 5250, 38000 Grenoble, France*

†Electronic supplementary information (ESI) available. See DOI: https://doi.org/10.1039/d4dt01499e

ligand through a C5–C6 bond. This feature distinguishes the 1,2,4-triazine from 1,2,4,5-tetrazines as there is no possibility of annealing phenanthroline or any other units to the tetrazine ring due to the absence of carbon–carbon bonds.

Synthesis

To compare the rate constants of our new complexes with published examples, we prepared complex **3** that has the same auxiliary ligand, cyclometallated 2-(2,4-difluorophenyl)-pyridine (Fig. 1). In addition to complex **3**, we also prepared complex **4** employing cyclometallated 2-phenylquinoline to achieve more red-shifted absorption and emission spectra that are desirable in luminescence bioimaging due to the improved penetrability of longer wavelength light.[17] Ligand **7** was synthesised in 48% yield in one step by the condensation of 1,10-phenanthroline-5,6-dione with *in situ* generated formamidrazone.[18,19] Complexes **3** and **4** were then derived by the reaction with the corresponding dichloro-bridged intermediates based on well-known chemistries in 40% and 26% yields, respectively. The complexes were isolated as chloride salts rather than more traditional, but less water-soluble, hexafluorophosphate analogues. The details of the synthesis and all analytical data can be found in the ESI.†

Kinetic studies

Strained bicyclo[6.1.0]nonyne (BCN) is a well-established bioorthogonal reagent that can be used as a dienophile in IEDDA reactions.[20] We had chosen BCN in our studies because the product of the IEDDA reaction with 1,2,4-triazine is an aromatic pyridine. The pyridine is part of the conjugated system of the metal complex and is beneficial for its luminescence properties. While there are several studies using TCO derivatives,[21–24] to the best of our knowledge, there are only two reports evaluating the kinetics of the reaction of 1,2,4-triaizine with BCN. In 2015, Webb *et al.* reported a second-order rate constant of 3.8×10^{-4} M^{-1} s^{-1} for the reaction of 3-substituted-1,2,4-triazine with benzoyl-protected BCN.[25] We previously reported that the coordination of 1,2,4-triazine to Ir(III) significantly boosts the reaction rates.[15] For example, the second order rate constant of ligand **6** was determined to be 0.059 M^{-1} s^{-1}, whereas the corresponding iridium complex **2** reacts with BCN two orders of magnitude faster, with a rate constant of 7.87 M^{-1} s^{-1} (Fig. 1).

BCN-C10 was selected as the dienophile for kinetics analysis. It is a crystalline compound and has a long storage lifetime compared to liquid or amorphous BCN derivatives. The second order rate constants for ligand **7** and complex **3** in reactions with **BCN-C10** were determined to be 0.0025 and 0.0081

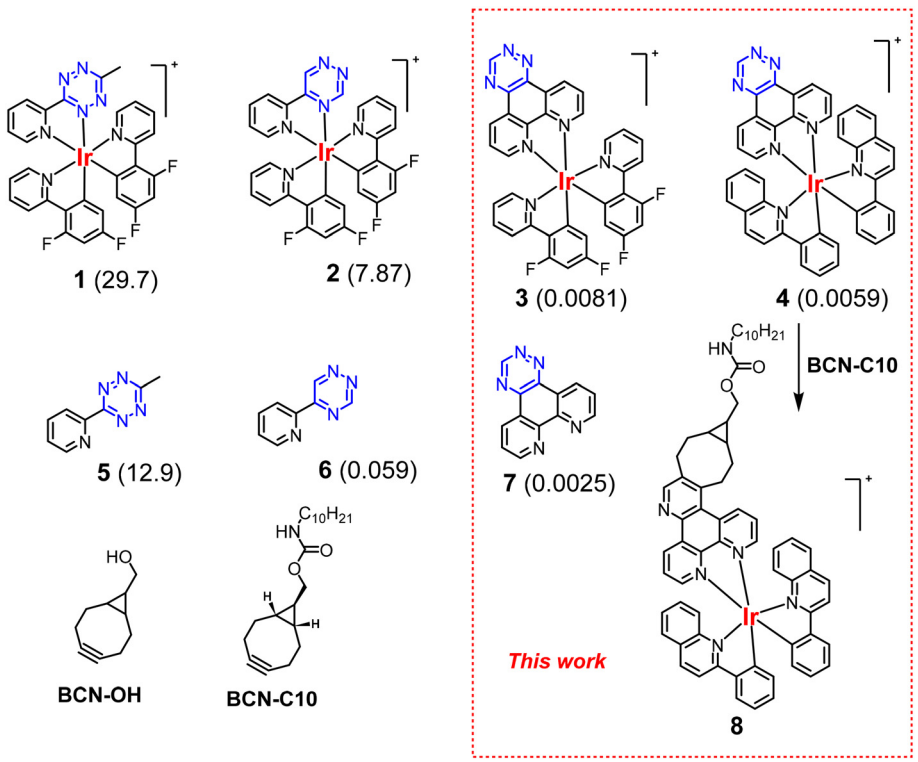

Fig. 1 Examples of iridium(III) complexes that demonstrate accelerated kinetics in the IEDDA reaction with BCN derivatives compared to the corresponding uncoordinated ligands. The second order rate constants k_2 (in M^{-1} s^{-1}) are shown in brackets. Reaction conditions: for **1** and **2**, CH_3CN : H_2O (1 : 1, v/v) at 25 °C and BCN-OH; for **2** and **6**, MeOH at 25 °C and BCN-OH; and for **3** and **7**, MeOH at 25 °C and **BCN-C10**. All IEDDA reactions are strongly luminogenic. Complex **8** was isolated for detailed analysis of the photophysical properties of the IEDDA reaction of complex **4** with BCN.

M^{-1} s^{-1} respectively, demonstrating that coordination to the Ir(III) metal ion facilitates the IEDDA reaction. However, the magnitude of the metal coordination effect in the **7**/**3** pair is much less profound than in **6**/**2** analogues (Fig. 1). Complex **4** showed a rate constant k_2 = 0.0059 M^{-1} s^{-1}. The rationale underpinning these observations is discussed below, with reference to computational analysis. The relatively low reaction rate of complexes **3** and **4** limits their bioorthogonal applications *in vivo* unless either reagent is present in large excess. Nevertheless, the reaction is still feasible for *in vitro* bioorthogonal chemistries, showing reaction rates of the same order as the well-known Staudinger ligation.

Computational analysis

DFT calculations were performed to gain insight into the underlying causes of the variation in the observed rate constants between complexes **2** and **3** and corresponding ligands **6** and **7**. Table 1 lists experimentally derived and calculated activation energies, ΔG_{act}, and the details of the calculated transition state geometries are given in the ESI.† Experimentally, both the directly bound triazine species, **2**/**6**, and the phenanthroline species, **3**/**7**, show a lowering of the activation energy on complexation, which is also reflected in the calculations. Additionally, the experimental trend of the phenanthroline species having higher activation energies than the equivalent directly bound triazine species is confirmed by the calculations, along with a larger drop in activation energy on complexation for the directly bound triazine than the phenanthroline.

The distortion–interaction model, which is routinely implemented to gain insight into the underlying influences on activation energies, was used for the calculated transition states of **6**, **2**, **7** and **3**, the results of which are shown in Fig. 2 (with tabulated values provided in the ESI, Table S1†). Differences in the distortion energies are evident, revealing that phenanthroline species **7** and **3** have larger distortion energies than triazines **6** and **2**. The distortion energy accounts for the main difference between the activation energies of ligands **7** and **6**, providing a rationale for the lower observed rate constant of **7**.

Table 1 Experimentally derived and calculated activation energies of reactions with BCN

	ΔG_{act}/kJ mol^{-1}	
Compound	Experimental	Calculated
Complex **2**	67.8[a]	70.0[c]
Ligand **6**	79.9[a]	99.8[c]
Complex **3**	85.0[b]	85.2[c]
Ligand **7**	87.9[b]	103.3[c]

[a] Determined in water/acetonitrile, 1/1. [b] Determined in methanol. [c] Calculated using a methanol solvent field.

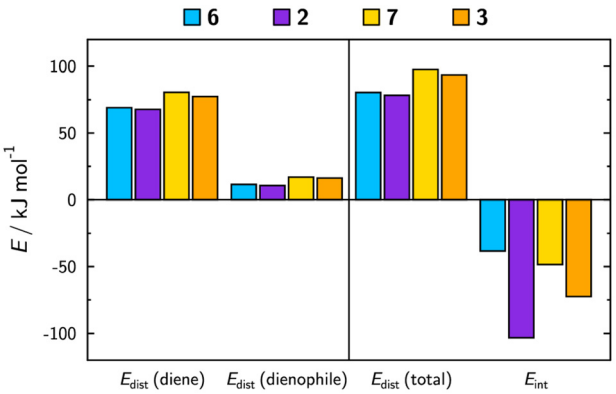

Fig. 2 Results of the distortion–interaction model for the calculated transition states of the reactions of ligands **6**, **7** and their Ir(III) complexes **2** and **3** with BCN.

The changes in activation energy on complexation are dominated by the calculated interaction energies, with complexes **2** and **3** exhibiting significantly more negative interaction energies than the free ligands, **6** and **7**. This decrease is significantly greater for **2** than for **3**, consistent with the experimentally derived activation energies.

Calculations of frontier orbital energies revealed a significant reduction of the energy gaps on complexation, providing further explanation for the faster reaction rates of the complexes (Fig. 3). The greater reduction in the energy gap on complexation for the directly bound triazine species compared to the phenanthroline provides a rationale for the greater increase in the experimentally observed reaction rate. The analysis of frontier orbital overlap integrals showed little difference between the directly bound triazine and phenanthroline on complexation, suggesting that the orbital energy differences have the most profound impact on the reaction rate. The details of the frontier molecular orbitals (Fig. S11†) and tabulated values (Table S2†) are provided in the ESI.†

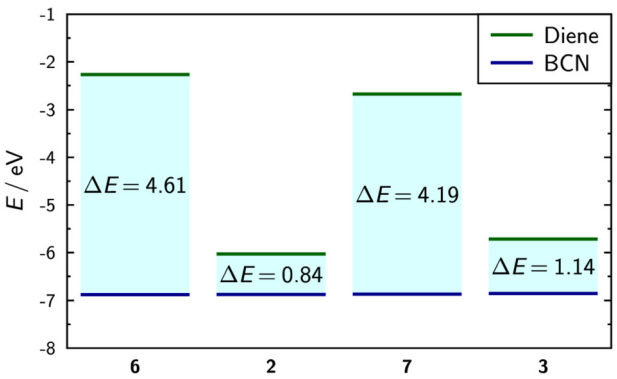

Fig. 3 Calculated frontier orbital energies and energy gaps between them for triazines **6**, **7**, **2**, and **3**, and BCN, determined from the calculated transition state geometries.

Photophysical properties

In bioimaging, luminogenic probes that 'switch on' after binding are of great interest due to the absence of luminescent background signals from non-conjugated probes, thereby eliminating the need for washing steps prior to imaging. While both complexes **3** and **4** showed strong luminogenic behaviour upon reaction with BCN, the shorter wavelength spectral profile of complex **3** rendered it largely unsuitable for bioimaging due to overlap with tissue autofluorescence and the limited availability of excitation sources in this region. Therefore, as the spectral profile of complex **4** demonstrated absorption at 488 nm, a commonly utilised wavelength for bioimaging, this complex was carried forward for further experimentation. To better understand changes in photophysical properties before and after the click reaction, complex **8** was isolated following the IEDDA reaction (Fig. 1) with **BCN-C10**. It should be noted that both complex **8** and **BCN-C10** derivatives are chiral and a mixture of stereoisomers is formed during the reaction. The triazine complex **4** is only very weakly emissive with a maximum at 593 nm in CH_2Cl_2, so no emission quantum yield could be estimated (*i.e.* $\Phi < 0.01$). In contrast, the product of the reaction, complex **8**, is highly emissive in deaerated EtOH ($\Phi = 0.23$) and CH_2Cl_2 ($\Phi = 0.65$) with emission maxima at 563 nm and 559 nm, respectively (ESI†). The lifetimes of emission are in the μs range and the complex is sensitive to the presence of oxygen ($k[O_2] = 0.31–0.61 \times 10^9$/L mol^{-1} s, in EtOH and CH_2Cl_2, respectively). The emission is slightly sensitive to the solvent polarity with a 4 nm (~194 cm^{-1}) bathochromic shift from CH_2Cl_2 to EtOH. Furthermore, at low temperature in a glassy solution in benzonitrile, complex **8** displays a structured emission accompanied by a small bathochromic shift (see the ESI†). Thus, the emission can be attributed to the radiative deactivation of a mixture of ^{3}IL/^{3}MLCT excited states to the ground state. Such interplay between excited states is well documented in cyclometallated iridium(III) complexes. The photophysical parameters and emission profile, *i.e.* λ_{em} and Φ, are highly similar to those observed for similar complexes with a phenanthroline ancillary ligand and 2-phenylquinoline as the cyclometallating ligand (Table 2).[26]

The ability of complex **8** to sensitize cytotoxic singlet oxygen was measured by a comparative method using phenalenone ($\phi_\Delta(CHCl_3) = 0.97 \pm 0.02$) as a reference.[27] The quantum yield of $^1O_2$ generation was found to be 0.68. The $^1O_2$ species facilitate cell death through oxidation of surrounding biomolecules, leading to the production of cytotoxic agents. Usually, cell death occurs through the initiation of apoptotic and necrotic pathways, and less frequently through oncosis or ferroptosis, all of which are mechanisms that underpin PDT for the treatment of cancer.[28,29]

The viability of utilising brightly luminescent complex **8** for bioimaging applications using a 488 nm excitation source was first assessed through flow cytometry analysis. Initial experiments indicated that the treatment of T lymphocyte Jurkat cells (ATCC® TIB-152™) with 1 μM solution of complex **8** in PBS buffer led to uptake of the complex by 97% of the cells within 30 minutes (ESI†), confirming that complex **8** is capable of staining live mammalian cells *in vitro*. Complex **8** was next evaluated for its potential use as a cellular stain using an immortalised cervical epithelial cell line, HeLa. These cells were first incubated with complex **8** and subsequently counterstained with DAPI, a very commonly used nucleus stain. Comparison between the luminescence signal from complex **8** and the fluorescent DAPI signal revealed that complex **8** demonstrates intracellular localisation (Fig. S17†). Further staining of HeLa cells using the membrane potential-dependent mitochondrial stain, MitoSpy Red, following incubation with complex **8** revealed co-distribution of the two signals, suggesting that complex **8** may localise to the mitochondria (Fig. S18†). Superimposition of images collected through both the channel used for complex **8** (488 nm) and the 561 nm channel was possible due to the lack of spectral overlap between the two emissive compounds.

"Chemistry on the complex" to prepare luminescent antibody conjugates

Amine-reactive luminescent metal complexes[30] can be used to label a variety of biomolecules, such as antibodies.[31] However, the amine-reactive groups are unstable in solution and have a tendency to degrade over time. In a 'chemistry on the complex' approach, the amine-reactive metal complex was synthesised through an *in situ* reaction of the triazine complex with the amine-reactive BCN derivative, prior to bioconjugation (Scheme 1). Such an approach is very convenient for testing libraries of novel Ir(III) complexes in the search for the most efficient luminescent probes. Triazine complex **3** was added to the amine-reactive **BCN-PNP** and incubated overnight at 50 °C to synthesise amine-reactive complex **9** (Scheme 1). The IEDDA

Table 2 Selected photophysical properties

Complex	Solvent	λ_{em}/nm	$\Phi^{a,b}$ [air]	τ^b/μs [air]	k_r 10^5/s^{-1}	Σk_{nr} 10^5/s^{-1}	$k[O_2]^c$ 10^9/L mol^{-1} s^{-1}	$\Phi_\Delta{}^d$
8	CH_2Cl_2	559^e, 585	0.65 [0.15]	2.50 [0.55]	2.6	1.4	0.61	0.68
8	EtOH	563^e, 588	0.23 [0.13]	1.20 [0.71]	1.9	6.42	0.31	—
4	CH_2Cl_2	562, 593^e	<0.01	—	—	—	—	—

[a] $Ru(bpy)_3{}^{2+}$ in air equilibrated CH_3CN was used as a reference. [b] In deaerated solution, unless otherwise mentioned. [c] With $[O_2] = 2.2$ mM in dichloromethane. [d] Determined in an air equilibrated solution of $CHCl_3$, using perinaphthenone as a standard in $CHCl_3$. [e] The most intense band.

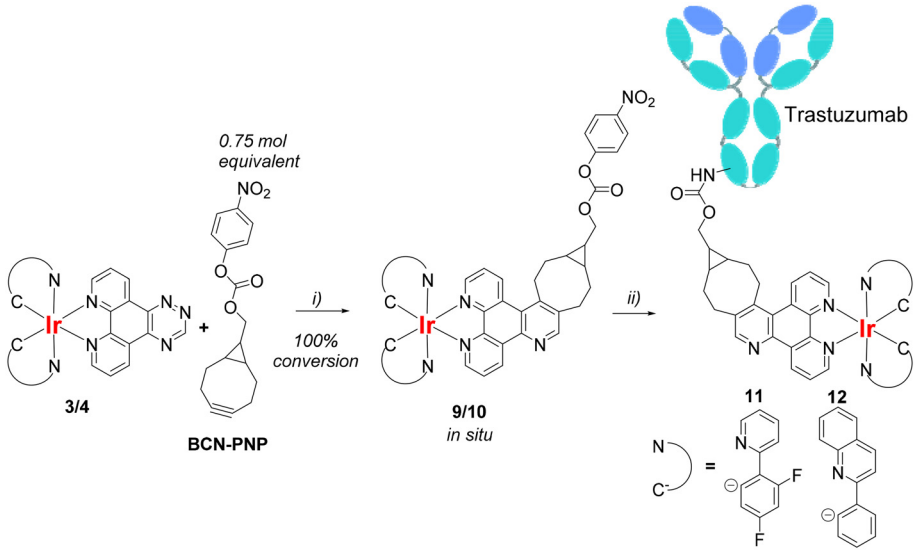

Scheme 1 *In situ* preparation of amine-reactive iridium(III) complexes **9** and **10** and their conjugation with trastuzumab. Reaction conditions: (i) DMSO-D_6 (for **3**) or DMSO (for **4**), 50 °C, and 16 hours; (ii) 30 mol equivalents of complex **9** or **10**, trastuzumab (1 mol eq.), 0.1 M $NaHCO_3$ (pH = 8.3), 37 °C, and 1 hour; yield of purified conjugate **11** (50%) and **12** (30%); and degree of labelling **11** (1.7) and **12** (2.3).

reaction was performed in an NMR tube using DMSO-d6 as the solvent, facilitating both the monitoring of the reaction and the preparation of the amine-reactive Ir(III) complex for subsequent bioconjugation. DMSO is routinely utilised to dissolve fluorophores for antibody labelling due to the relatively high tolerance of DMSO by antibodies, documented to be approximately 10% v/v. An excess of **3** with respect to **BCN-PNP** was used to make sure that only amine-reactive complex **9** conjugated to the antibody. ^{1}H NMR confirmed that the reaction had run to completion (100% conversion with respect to **BCN-PNP**) due to the absence of signals of **BCN-PNP** to give a mixture of 74% of desired product **9** with the remaining portion being starting complex **3**. However, the presence of the triazine starting material is not problematic as it is incapable of reacting with an antibody due to the lack of the amine-reactive handle and is easily removed after the conjugation reaction during protein purification.

Informed by NMR data confirming the successful formation of complex **9**, complex **10** was next synthesised through the same methods by combining complex **4** with **BCN-PNP**, although this reaction was carried out in non-deuterated DMSO. As the resulting click product is luminogenic, the reaction can be monitored visually through observation of the reaction tube under a UV lamp (λ_{ex} 365 nm) (Fig. S19†). The solutions containing the *in situ* generated amine-reactive complexes were then used in this unmodified condition for conjugation to the HER2-specific immunoglobulin G (IgG) antibody, trastuzumab. Luminescent iridium(III) immunoconjugates **11** and **12** were synthesised through stochastic modification of the endogenous lysine residues in the antibody structure *via* amide bond formation at ε-amino positions in a bicarbonate buffer (Scheme 1). A 30-fold molar excess of amine-reactive complex **9**/**10** yielded degrees of labelling (DOLs) of 1.7 ± 0.3 and 2.3 ± 0.8, respectively, which are determined using UV-vis measurements of the purified conjugates. The long wavelength absorption and emission characteristics of conjugate **12** are very similar to those of model compound **8**.

Antibody conjugates were analysed by sodium dodecyl sulfate polyacrylamide gel electrophoresis (SDS-PAGE) to qualitatively validate bioconjugation products **11** and **12** (Fig. 4). The colocalisation of the luminescence from the iridium(III) immunoconjugates (red) with the fluorescence from the stained antibody at 150 kDa (green) indicates the attachment of the iridium(III) complex to trastuzumab.

In vitro evaluation of the immunoconjugates on breast cancer cell lines and the potential application of the conjugates for photodynamic therapy will be reported in due course.

Cytotoxicity and bioorthogonal reactivity of the complexes

Bioorthogonality requires compounds to be stable and non-toxic at experimentally-relevant concentrations. Testing the stability of complexes **3** and **4** in PBS at pH 7.4 (the pH of the cell culture media) and at 37 °C showed no degradation even after 48 h of incubation (Fig. S21†). The cytotoxicity of iridium complexes **3** and **4** has been investigated on human melanoma A-375 cells and non-cancer HFF-1 cells (human foreskin fibroblasts) by MTT cell viability assays. The results obtained after 24 h, 48 h and 72 h of incubation are summarized in Table 3.

IC_{50} values determined for both complexes on A-375 cancer cells indicated higher toxicity for **4** compared to **3** after 24, 48 and 72 h of incubation. Interestingly, complex **4** demonstrated significantly lower toxicity on non-cancerous HFF-1 cells compared to the melanoma A-375 cell line (Table 3). However, for

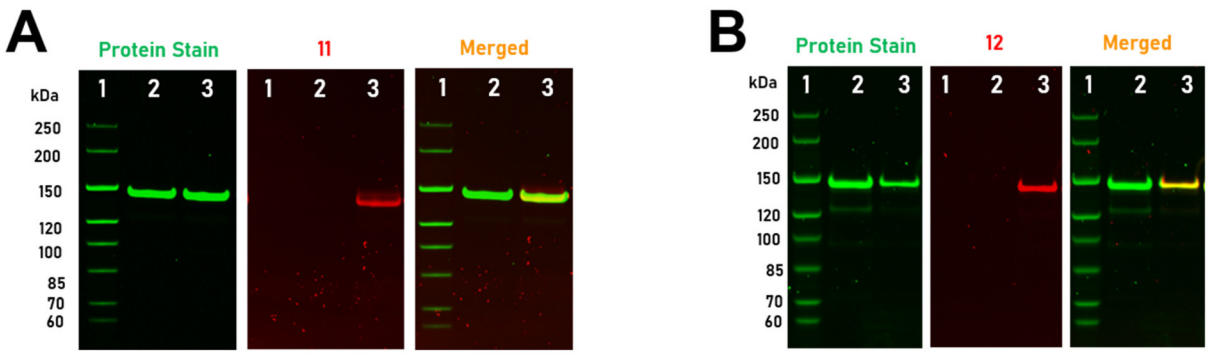

Fig. 4 SDS-PAGE of iridium complex immunoconjugates. (A) Unmodified trastuzumab (lane 2) and immunoconjugate **11** (lane 3) compared to a protein ladder. (B) Unmodified trastuzumab (lane 2) and immunoconjugate **12** (lane 3) compared to a protein ladder. The gel was stained with Coomassie Fluor™ Orange and analysed through fluorescence imaging. The luminescence of the Ir(III) complex was recorded using excitation $\lambda_{ex.}$ = 302 nm collecting emission in the range of $\lambda_{em.}$ = 535–645 nm.

Table 3 IC_{50} values (μM) for complexes **3** and **4**. The concentration leading to a 50% decrease in cell viability compared to untreated cells (IC_{50}) was determined on melanoma A-375 cells and human fibroblasts HFF-1. Triplicate data are shown as mean ± SD of three independent experiments

IC_{50} (μM)						
	A-375			HFF-1		
Complex	24 h	48 h	72 h	24 h	48 h	72 h
3	23.9 ± 0.1	24.7 ± 0.4	24.9 ± 0.8	24.9 ± 0.7	21.1 ± 0.4	15.4 ± 0.3
4	3.6 ± 0.5	1.9 ± 0.2	1.9 ± 0.3	9.1 ± 0.1	6.4 ± 0.3	5.7 ± 0.8

complex **3**, similar cytotoxic properties were determined on both cell lines (Table 3). Increased toxicity towards cancer cells over healthy cells is highly desirable for compounds used for therapeutic or diagnostic applications.

To demonstrate the bioorthogonal reactivity and luminogenic behaviour of complex **4** we employed metabolic labelling using BCN-modified Ac_4Man*N*BCN.[32] This modified monosaccharide has been reported to be efficiently metabolized *via* the sialic acid biosynthesis pathway, thus leading to a high level of reporter group expression on the surface of cell organelles.[33] Once expressed into the cell, the BCN group can then react *via* the IEDDA reaction with triazine metal complex **4**. This bioorthogonal ligation will be accompanied by the appearance of luminescence. Complex **4** was selected for this experiment as this click product is excitable using a 488 nm laser, due to similarities between its absorption spectrum and that of model compound **8**. Therefore, to investigate the luminescence behaviour of triazine iridium complex **4** following a click reaction, A-375

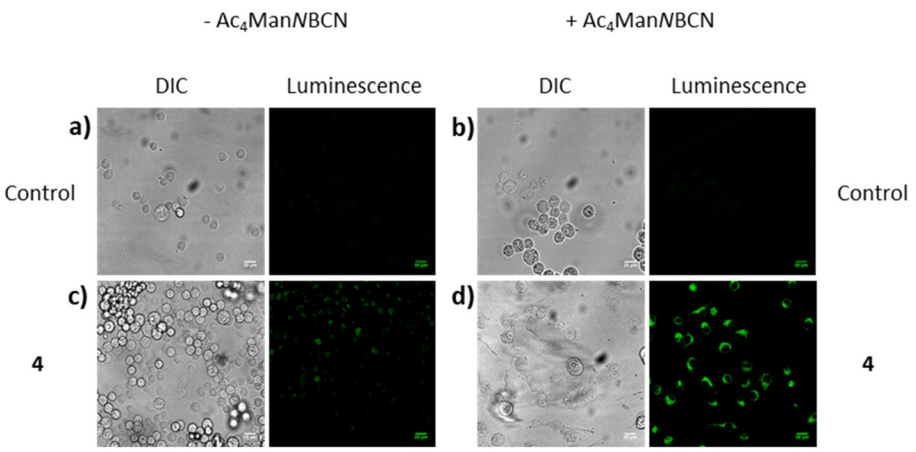

Fig. 5 Confocal fluorescence microscopy images of A-375 cells after treatment with Ac_4Man*N*BCN and **4**. (a) Cells without treatment. (b) Cells incubated with Ac_4Man*N*BCN (50 μM). (c) Non-BCN-labelled cells treated with 10 μM **4**. (d) Cells incubated with Ac_4Man*N*BCN (50 μM) and then treated with 10 μM **4**. Differential Interference Contrast (DIC) is shown in the left column and luminescence is shown on the right for each condition.

cells were incubated with 50 μM BCN-sugar for 48 h prior to treatment with 10 μM complex **4** for 30 min at 37 °C, and subsequently imaged by fluorescence confocal microscopy. Cells without treatment or treated only with $Ac_4ManNBCN$ or complex **4** were implemented as negative controls. Strong luminescence was detected for cells treated successively with $Ac_4ManNBCN$ and **4** (Fig. 5d), while much weaker fluorescence was measured for cells not pre-incubated with BCN-sugar (Fig. 5c). Analysis by fluorescence-activated cell sorting (FACS) of cells treated with increasing concentrations of **4** (0.5 to 50 μM) showed an increase of luminescence signals for cells pre-labelled with $Ac_4ManNBCN$ (Fig. S20†). The control cells without pre-labelling with $Ac_4ManNBCN$ did not show luminescence. These results demonstrate successful $Ac_4ManNBCN$ glycometabolism by A-375 cells, as well as a bioorthogonal luminogenic reaction to visualise metabolically glycosylated cells using complex **4**.

Conclusion

Phenanthroline iridium(III) complexes containing an annealed 1,2,4-triazine ring were prepared for the first time. Such annealing of the click group is unique to 1,2,4-triazines and it is not possible in 1,2,4,5-tetrazines. The inverse electron demand Diels–Alder reaction with BCN derivatives was found to be strongly luminogenic with the increase of quantum yield from a nearly non-emissive state to 13% in aerated ethanol solution. As the 1,2,4-triazine ring is not directly coordinated to the metal centre, the IEDDA reaction is facilitated to a lesser extent in comparison with directly coordinated 1,2,4-triazines. The reaction is nevertheless a convenient tool for preparing luminescent bioconjugates as well as for *in vitro* bioorthogonal luminescent cell labelling. Many other phenanthroline metal complexes containing an annealed 1,2,4-triazine ring can be envisaged as click reagents in IEDDA reactions offering an efficient pathway for the functionalisation of biomolecules and other substrates with metal-based properties.

Data availability

The authors declare that the data supporting the findings of this study are available within the paper and its ESI files.† Should any raw data files be needed in another format they are available from the corresponding author upon reasonable request.

Conflicts of interest

There are no conflicts to declare.

Acknowledgements

NB acknowledge support from the "Investissements d'avenir" program Glyco@Alps (ANR-15-IDEX-02) and Labex Arcane/CBH-EUR-GS (ANR-17-EURE-0003).

References

1 Y. Chen, H. Jiang, T. Hao, N. Zhang, M. Li, X. Wang, X. Wang, W. Wei and J. Zhao, Fluorogenic Reactions in Chemical Biology: Seeing Chemistry in Cells, *Chem. Biomed. Imaging*, 2023, **1**(7), 590–619, DOI: **10.1021/cbmi.3c00029**.

2 A. W.-T. Choi, K. K.-S. Tso, V. M.-W. Yim, H.-W. Liu and K. K.-W. Lo, Modification of 1,2,4,5-tetrazine with cationic rhenium(I) polypyridine units to afford phosphorogenic bioorthogonal probes with enhanced reaction kinetics, *Chem. Commun.*, 2015, **51**(16), 3442–3445, DOI: **10.1039/C4CC09532D**.

3 J. Ohata, F. Vohidov, A. Aliyan, K. Huang, A. A. Marti and Z. T. Ball, Luminogenic iridium azide complexes, *Chem. Commun.*, 2015, **51**(82), 15192–15195, DOI: **10.1039/C5CC06099K**.

4 T. S.-M. Tang, H.-W. Liu and K. K.-W. Lo, Monochromophoric iridium(III) pyridyl–tetrazine complexes as a unique design strategy for bioorthogonal probes with luminogenic behavior, *Chem. Commun.*, 2017, **53**(23), 3299–3302, DOI: **10.1039/C7CC00427C**.

5 G.-X. Xu, E. C.-L. Mak and K. K.-W. Lo, Photofunctional transition metal complexes as cellular probes, bioimaging reagents and phototherapeutics, *Inorg. Chem. Front.*, 2021, **8**(20), 4553–4579, DOI: **10.1039/D1QI00931A**.

6 L. C.-C. Lee and K. K.-W. Lo, Luminescent and Photofunctional Transition Metal Complexes: From Molecular Design to Diagnostic and Therapeutic Applications, *J. Am. Chem. Soc.*, 2022, **144**(32), 14420–14440, DOI: **10.1021/jacs.2c03437**.

7 J. Zhou, J. Li, K. Y. Zhang, S. Liu and Q. Zhao, Phosphorescent iridium(III) complexes as lifetime-based biological sensors for photoluminescence lifetime imaging microscopy, *Coord. Chem. Rev.*, 2022, **453**, 214334, DOI: **10.1016/j.ccr.2021.214334**.

8 S. Tobita and T. Yoshihara, Intracellular and in vivo oxygen sensing using phosphorescent iridium(III) complexes, *Curr. Opin. Chem. Biol.*, 2016, **33**, 39–45, DOI: **10.1016/j.cbpa.2016.05.017**.

9 K. K.-W. Lo and K. Y. Zhang, Iridium(III) complexes as therapeutic and bioimaging reagents for cellular applications, *RSC Adv.*, 2012, **2**(32), 12069–12083, DOI: **10.1039/C2RA20967E**.

10 Y. Zhang, B.-T. Doan and G. Gasser, Metal-Based Photosensitizers as Inducers of Regulated Cell Death Mechanisms, *Chem. Rev.*, 2023, **123**(16), 10135–10155, DOI: **10.1021/acs.chemrev.3c00161**.

11 R. E. Daniels, L. K. McKenzie, J. R. Shewring, J. A. Weinstein, V. Kozhevnikov and H. E. Bryant, Pyridazine-bridged cationic diiridium complexes as potential dual-mode bioimaging probes, *RSC Adv.*, 2018, **8**(18), 9670–9676, DOI: **10.1039/C8RA00265G**.

12 Y. Osakada, G. Pratx, L. Hanson, P. E. Solomon, L. Xing and B. Cui, X-ray excitable luminescent polymer dots doped with an iridium(III) complex, *Chem. Commun.*, 2013, **49**(39), 4319–4321, DOI: **10.1039/C2CC37169C**.

13 Y. Fang, A. S. Hillman and J. M. Fox, Advances in the Synthesis of Bioorthogonal Reagents: s-Tetrazines, 1,2,4-Triazines, Cyclooctynes, Heterocycloheptynes, and trans-Cyclooctenes, *Top. Curr. Chem.*, 2024, **382**(2), 15, DOI: **10.1007/s41061-024-00455-y**.

14 X. Xu, S. Shabiti, X. Zhang, J. Zheng, N. Liang, Z. Wang, S. Yu, Y. Wang, S. Jiang, Z. Pan, *et al.*, Membrane-anchoring clickable Iridium(III) nanosonosensitizer in situ evokes PANoptosis for augmented tumor sono-immunotherapy, *Nano Today*, 2024, **56**, 102270, DOI: **10.1016/j.nantod.2024.102270**.

15 V. N. Kozhevnikov, M. E. Deary, T. Mantso, M. I. Panayiotidis and M. T. Sims, Iridium(III) complexes of 1,2,4-triazines as potential bioorthogonal reagents: metal coordination facilitates luminogenic reaction with strained cyclooctynes, *Chem. Commun.*, 2019, **55**(95), 14283–14286, DOI: **10.1039/C9CC06828G**.

16 M. Sims, S. Kyriakou, A. Matthews, M. E. Deary and V. N. Kozhevnikov, Catching up with tetrazines: coordination of Re(i) to 1,2,4-triazine facilitates an inverse electron demand Diels–Alder reaction with strained alkynes to a greater extent than in corresponding 1,2,4,5-tetrazines, *Dalton Trans.*, 2023, **52**(31), 10927–10932, DOI: **10.1039/D3DT01451G**.

17 J. S.-Y. Lau, P.-K. Lee, K. H.-K. Tsang, C. H.-C. Ng, Y.-W. Lam, S.-H. Cheng and K. K.-W. Lo, Luminescent Cyclometalated Iridium(III) Polypyridine Indole Complexes—Synthesis, Photophysics, Electrochemistry, Protein-Binding Properties, Cytotoxicity, and Cellular Uptake, *Inorg. Chem.*, 2009, **48**(2), 708–718, DOI: **10.1021/ic801818x**.

18 G. R. Pabst, O. C. Pfüller and J. r. Sauer, The new and simple 'LEGO' system: Its application for the synthesis of 6-oligopyridyl-1,5,12-triazatriphenylenes, *Tetrahedron Lett.*, 1998, **39**(48), 8825–8828, DOI: **10.1016/S0040-4039(98)02044-9**.

19 H. Neunhoeffer and F. Weischedel, Synthese von Amidrazonen aus Amidinen, *Justus Liebigs Ann. Chem.*, 1971, **749**(1), 16–23, DOI: **10.1002/jlac.19717490104**.

20 J. Dommerholt, S. Schmidt, R. Temming, L. J. A. Hendriks, F. P. J. T. Rutjes, J. C. M. van Hest, D. J. Lefeber, P. Friedl and F. L. van Delft, Readily Accessible Bicyclononynes for Bioorthogonal Labeling and Three-Dimensional Imaging of Living Cells, *Angew. Chem., Int. Ed.*, 2010, **49**(49), 9422–9425, DOI: **10.1002/anie.201003761**.

21 V. Šlachtová, V. Motornov, P. Beier and M. Vrabel, Bioorthogonal Cycloadditions of C3-Trifluoromethylated 1,2,4-Triazines with trans-Cyclooctenes, *Chemistry*, 2024, e202400839, DOI: **10.1002/chem.202400839**, From NLM.

22 D. N. Kamber, Y. Liang, R. J. Blizzard, F. Liu, R. A. Mehl, K. N. Houk and J. A. Prescher, 1,2,4-Triazines Are Versatile Bioorthogonal Reagents, *J. Am. Chem. Soc.*, 2015, **137**(26), 8388–8391, DOI: **10.1021/jacs.5b05100**.

23 S. J. Siegl, R. Dzijak, A. Vazquez, R. Pohl and M. Vrabel, The discovery of pyridinium 1,2,4-triazines with enhanced performance in bioconjugation reactions, *Chem. Sci.*, 2017, **8**(5), 3593–3598, DOI: **10.1039/C6SC05442K**.

24 Z. Chen, N. Ren, X. Ma, J. Nie, F.-G. Zhang and J.-A. Ma, Silver-Catalyzed [3 + 3] Dipolar Cycloaddition of Trifluorodiazoethane and Glycine Imines: Access to Highly Functionalized Trifluoromethyl-Substituted Triazines and Pyridines, *ACS Catal.*, 2019, 4600–4608, DOI: **10.1021/acscatal.9b00846**.

25 K. A. Horner, N. M. Valette and M. E. Webb, Strain-Promoted Reaction of 1,2,4-Triazines with Bicyclononynes, *Chem. – Eur. J.*, 2015, **21**(41), 14376–14381, DOI: **10.1002/chem.201502397**.

26 B. Liu, L. Lystrom, S. L. Brown, E. K. Hobbie, S. Kilina and W. Sun, Impact of Benzannulation Site at the Diimine (N^N) Ligand on the Excited-State Properties and Reverse Saturable Absorption of Biscyclometalated Iridium(III) Complexes, *Inorg. Chem.*, 2019, **58**(9), 5483–5493, DOI: **10.1021/acs.inorgchem.8b03162**.

27 R. Schmidt, C. Tanielian, R. Dunsbach and C. Wolff, Phenalenone, a universal reference compound for the determination of quantum yields of singlet oxygen $O_2(1\Delta g)$ sensitization, *J. Photochem. Photobiol., A*, 1994, **79**(1), 11–17, DOI: **10.1016/1010-6030(93)03746-4**.

28 H. Yuan, Z. Han, Y. Chen, F. Qi, H. Fang, Z. Guo, S. Zhang and W. He, Ferroptosis Photoinduced by New Cyclometalated Iridium(III) Complexes and Its Synergism with Apoptosis in Tumor Cell Inhibition, *Angew. Chem., Int. Ed.*, 2021, **60**(15), 8174–8181, DOI: **10.1002/anie.202014959**.

29 E. Ortega-Forte, S. Hernández-García, G. Vigueras, P. Henarejos-Escudero, N. Cutillas, J. Ruiz and F. Gandía-Herrero, Potent anticancer activity of a novel iridium metallodrug via oncosis, *Cell. Mol. Life Sci.*, 2022, **79**(10), 510, DOI: **10.1007/s00018-022-04526-5**.

30 I. S. Kritchenkov, D. D. Zhukovsky, A. Mohamed, V. A. Korzhikov-Vlakh, T. B. Tennikova, A. Lavrentieva, T. Scheper, V. V. Pavlovskiy, V. V. Porsev, R. A. Evarestov, *et al.*, Functionalized Pt(II) and Ir(III) NIR Emitters and Their Covalent Conjugates with Polymer-Based Nanocarriers, *Bioconjugate Chem.*, 2020, **31**(5), 1327–1343, DOI: **10.1021/acs.bioconjchem.0c00020**.

31 T. U. Connell and P. S. Donnelly, Labelling proteins and peptides with phosphorescent d6 transition metal complexes, *Coord. Chem. Rev.*, 2018, **375**, 267–284, DOI: **10.1016/j.ccr.2017.12.001**.

32 W. Li, H. Pan, H. He, X. Meng, Q. Ren, P. Gong, X. Jiang, Z. Liang, L. Liu, M. Zheng, *et al.*, Bio-Orthogonal T Cell Targeting Strategy for Robustly Enhancing Cytotoxicity against Tumor Cells, *Small*, 2019, **15**(4), 1804383, DOI: **10.1002/smll.201804383**.

33 L. Zhou, C. Liu, Y. Zheng, Z. Huang, X. Zhang and Y. Xiao, Bioorthogonal Toolbox for Monitoring Nitric Oxide in Targeted Organelles of Live Cells and Zebrafishes, *Anal. Chem.*, 2022, **94**(45), 15678–15685, DOI: **10.1021/acs.analchem.2c02768**.